J Fusion Energ
DOI 10.1007/s10894-010-9372-1

ORIGINAL RESEARCH

Characterizing Plasma Focus Devices—Role of the Static Inductance—Instability Phase Fitted by Anomalous Resistances

S. Lee · S. H. Saw · A. E. Abdou · H. Torreblanca

Abstract Plasma focus devices with low static inductance L_0 (type *T1*) are found to be well modeled by the 5-phase Lee code; whereas those with high L_0 (type *T2)* are found to have an extended dip *ED* beyond the regular dip *RD* modeled by the code. Differentiating factors based on inductance and inductive energy ratios are found and the physics explained. To model type *T2*'s, anomalous resistance terms are proposed extending the model to 6 phases. These anomalous resistance terms represent the plasma instabilities that occur during and after the pinch phase. The fitted terms are experimental results derived from the measured current waveform. An example is tested to validate the method.

Keywords Plasma focus · Plasma focus modeling · Lee model code · Plasma focus classification · Plasma focus inductance · Plasma focus energy distributions · Plasma focus instability phase

S. Lee (✉) · S. H. Saw
INTI International University, 71800 Nilai, Malaysia
e-mail: leesing@optusnet.com.au

S. Lee · S. H. Saw
Institute for Plasma Focus Studies, 32 Oakpark Drive, Chadstone, VIC 3148, Australia

S. Lee
National Institute of Education, Nanyang Technological University, Singapore 637616, Singapore

A. E. Abdou
Kansas State University, Manhattan, KS 66506, USA

H. Torreblanca
Intel Corporation, Hillsboro, OR 97124, USA

Introduction

The Lee model code couples plasma and current sheath dynamics, thermodynamics and radiation with electric circuit equations to simulate the electrodynamic properties of the plasma focus [1–4]. To simulate any Mather-type plasma focus device, the link between the computation and physical reality is by means of fitting the computed current waveform to a measured current waveform using four model parameters f_m, f_c and f_{mr} and f_{cr}; the former two being to account for non-perfect mass swept up [5] and current drive due to all physical and machine processes in the axial phase, and likewise the latter two for the radial phases. The model code includes five phases: an axial phase treated as snow-plow like**;** a radial inwards shock phase using a slug model**;** a radial reflected shock phase with the reflected shock moving radially outwards until it hits the radially incoming current sheath 'piston'**;** followed by phase 4, a slow compression radiative pinch phase with the radiative loss of energy coupled into the compression of the pinch. A final phase 5, with large column axial expansion, is modeled to complete the current waveform evolution [6–14]. The transition from phase 4 to phase 5; is not modeled but simply taken as a sudden expansion of the pinch from a small pinch radius (typically with a radius about 0.1 times the anode radius) to a large column taken to have the radius of the anode [2]. The modelling of the radial phases and the transition from phase 4 to phase 5 is in conformity with streak photo studies of which a representative is shown in Fig. 1 [15, 16].

The radial implosion starts from near the left edge of the photograph. The light emitting plasma starting at the edge of the anode face, streaks inwards symmetrically (phase 2, the radial imploding shock phase) until the shock front implodes axisymmetrically onto the axis. As can be seen

Published online: 25 December 2010

Fig. 1 Streak photograph of UMDPF1. The axis of symmetry is the horizontal line across the vertical middle of the photograph. *Vertical scale* is distance, being 25 mm across the whole vertical length of the photograph. *Horizontal scale* is time, being 300 ns across the horizontal length of the photograph

from the photograph the rear edge of the imploding plasma which we take to be the magnetic piston then forms the boundary of the plasma pinch column with a time duration of around 30 ns. During this period the pinch radius first reduces slightly (phase 3, the reflected shock phase) then starts expanding slightly (phase 4, the pinch phase); then all of a sudden the bright luminosity disappears; and within nanoseconds the streak photograph indicates that a much lower luminosity has spread across the vertical extent of the photograph (phase 5, the large column axial phase). The time scale of the disappearance is shorter than the time scale of the implosion and the pinch.

Fitting Plasma Focus Devices Using the Lee Code—Low Inductance Ones Fit Well Overall, High Inductance Ones Fit Only the First Part With the Measured Current Continuing Beyond the Modeled Dip

The Lee code does not model the transition from Phase 4 to Phase 5. Nevertheless, it has been found to be adequate for modelling all the well-known plasma focus with low static inductance L_0 [2–14] which we have fitted; in the sense that the computed current traces can be fitted to the measured current trace by adjustment of the model parameters f_m, f_c, f_{mr} and f_{cr}. This has been the case for the PF1000, PF400J, NX1, NX2, DPF78, Poseidon [17], FMPF1 [18], FN-II [9]. Some examples are shown in Figs. 2, 3, 4.

Amongst the well-published plasma focus devices only the UNU/ICTP PFF [19–24] which has relatively higher L_0 of 110 nH presented less certainty in the fitting. This was due to a very small computed current dip and a measured current dip that has always been masked by very large oscillations taken to be noise; although when operated in unusually low pressure regime, a clear discrepancy was noted between the computed and measured current trace [25].

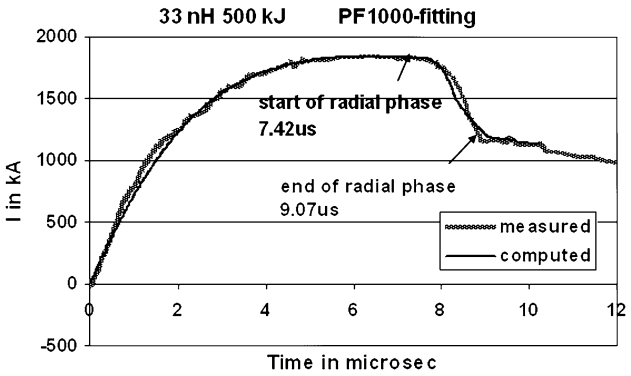

Fig. 2 Computed current trace of PF1000 fitted to the measured current trace

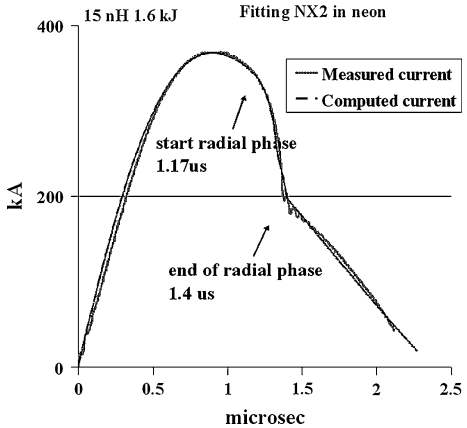

Fig. 3 Computed current trace of NX2 fitted to the measured current trace

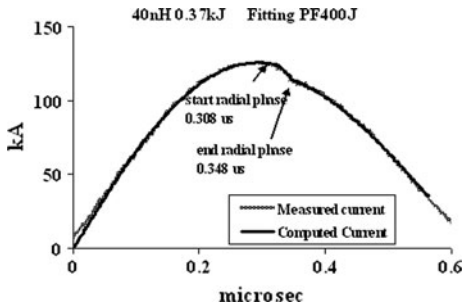

Fig. 4 Computed current trace of PF-400 J fitted to the measured current trace

Recently a current trace from the newly commissioned KSU DPF (Kansas State University Dense Plasma Focus) [26] which has an even higher L_0, was obtained by numerically integrating the output of a d*I*/d*t* coil. An analysis of the frequency response of the coil system and the DSO signal acquisition system showed that noise frequencies below 200 MHz were removed by the numerical integration. The resultant waveform is clean and clearly shows an extended current dip with good depth and

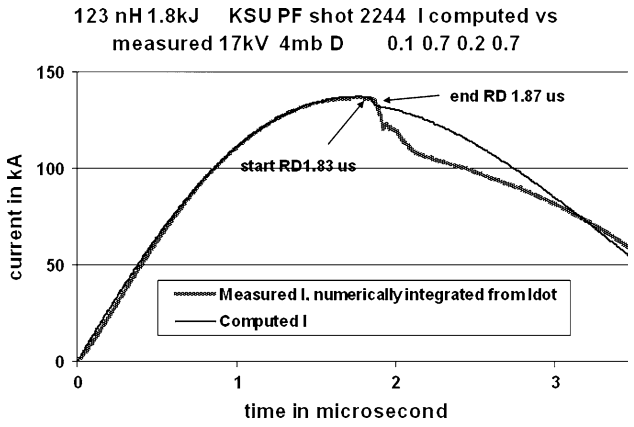

Fig. 5 Computed current trace (*lighter trace*) with best attempt to fit to the measured current trace (*darker trace*)

duration (see Fig. 5, the darker trace). The KSU DPF shows very consistent operation with more than 95% of the shots showing current dips with similar depth and duration.

Following the usual procedure of the Lee model code, an attempt was made to fit the computed current trace with the measured. The computed current trace has only a small dip as is characteristic of the computed current dip of a device with large static inductance L_0. All possible adjustments were made to the model parameters but the computed current dip could not be made to fit the whole measured current dip. The best fit is shown in Fig. 5; which shows that the computed dip does fit the first small part of the measured current dip. But the measured dip continues on in both depth and duration far beyond the computed dip.

Factors Distinguishing the Two Types of Plasma Focus Devices

The code models the electrodynamic situation using the slug model and a reflected shock for the radial phase, ending the radial phase in phase 4. Let's call the radial phase modeled in that manner as the REGULAR radial phase. This REGULAR radial phase, in increasing sharply the inductance of the system (constituting also a dynamic resistance [8]) causes a dip on the current trace. Call this the regular dip *RD*. At the end of the REGULAR radial phase experimental observations point to another phase [15, 25, 27], which we shall call phase 4a, (i.e. after phase 4, but before the final axial phase, called phase 5), of 'instabilities' manifesting in anomalous resistance. These effects would also extract energy from the magnetic field and hence produce further current dips. These effects are not modeled specifically in the code. Call this the extended current dip *ED*.

However, it may be argued that as long as the model parameters can be stretched sufficiently to have the computed current dip agree with the measured current dip, then in a gross sense, the modelling is energetically and mass-wise equivalent to the physical situation. Then the resulting gross characteristics from the model would give a fair representation of the actual plasma properties, even though the model has not specifically modeled *ED*. In other words *RD* is able to be stretched to also model *ED*, with equivalent energetics and mass implications. Whether *RD* can be stretched sufficiently to cover *ED* depends on the relative sizes of the two effects. If *RD* is already a big dip, then this effect may dominate and it is more likely that *RD* may be stretched sufficiently to cover the less prominent *ED*. If *RD* is only a miniscule dip and *ED* is a big dip, then it is unlikely that the *RD* can be stretched enough to encompass the *ED*.

We attempt to establish criteria for discriminating the types. Noting that generally a plasma focus with small L_0, for example the PF1000 with $L_0 = 33$ nH, exhibits a large computed *RD* (see Fig. 2 and also Figs. 3 and 4) whereas a plasma focus with a large L_0, for example the KSU PF with $L_0 = 123$ nH, exhibits a small computed *RD* (see Fig. 5) we suspect that it has something to do with the inductance L_0, or the ratio of L_0 with various inductances inherent in the system. We carried out several series of numerical experiments with various configurations similar to existing plasma focus devices, varying the value of L_0 in each series and looking at the effect on remnant energies at the end of the *RD*. Some interesting conclusions may be drawn from a tabulation, such as in Table 1.

Computing the values of these two quantities for PF1000, Poseidon, DPF78, NX2, PF400J, FMPF-1, FNII and UNU/ICTPPFF and KSU PF, we have a range of devices from very big (MJ) to rather small (sub kJ) of

Table 1 Classification of plasma focus machines (D_2 operation)

PF name	L_0 (nH)	C_0 (μF)	I_{peak} (kA)	R_L	R_{EL}	RD dip (%)	Type
Poseidon	17.7	156	3205	0.9	2.5	32	*T1*
PF1000	33.5	1332	1845	1	1.6	34	*T1*
DPF78	55	17.2	869	4.1	12.8	11	*T1*
FN-II	75	7.5	309	4.3	8.5	10	*T1*
FMPF1	31	2.4	81	6.9	8.6	14.5	*T1*
PF-400 J	40	1	126	8.8	17.3	8	*T1*
UNUICTP	110	30	163	16.7	29.5	1.9	*T2*
KSU	123	12.5	137	21.4	40	1.5	*T2*

We considered the inductance ratio $R_L = (L_0 + L_a)/L_{pinch}$ where L_{pinch} is the inductance of the focus pinch at the end of the REGULAR radial phase, L_0 the bank static inductance and L_a the inductance of the axial part of the focus tube. We also considered the remnant energy ratio $R_{EL} = (E_{L0} + E_{La})/E_{Lpinch}$ where E_{L0} = energy stored in L_0 at end of the *RD*, E_{La} = energy stored in L_a at end of the *RD* and E_{Lpinch} = energy stored inductively in the pinch at end of *RD*

which we have well documented fittings. These are shown in Table 1 for operation in D_2. For other gases there are not many examples. We are able to compile Table 2 for operation in Ne.

Generally we see the trend that the smaller is the ratio R_L, the bigger is the regular current dip (*RD*). When this ratio is large (primarily due to a large L_0 in the numerator), like in the case of KSU PF, the REGULAR radial phase RD is miniscule. Likewise, the trend is also observed for the ratio R_{EL}. The smaller this energy ratio, the bigger is the current dip.

On the basis of these two ratios we have divided the plasma focus devices in Tables 1 and 2 into two types: T1 and T2. Type T1 are for plasma focus devices with relatively small L_0 with large RD's and with relatively small ratios R_L and R_{EL}. These T1 focus devices are well-fitted using the Lee model code. The computed current traces (with radial phase computed only as a regular dip RD) are well-fitted to the whole measured current trace. Type *T2* are for plasma focus devices with relatively large L_0 with small *RD*'s and with relatively large ratios of R_L and R_{EL}. These *T2* focus devices are not well-fitted using the Lee model code. The computed current trace shows only a small dip which is fitted to the first portion of the measured current dip; but the measured current dip has an extended portion which is not well-fitted using the five-phase Lee model code.

Next we note that the magnetic energy density per unit mass at the start of the radial phase is the same across the whole range of devices [28]. Thus, *T1* with a big *RD* drops the current a lot and strongly depletes the magnetic energy per unit mass at the end of the RD, leading to a small *ED*. Consequently *T1* are completely fitted using a model that computes only the *RD*, stretching the model parameters until the large *RD* covers also the small *ED*. Conversely a *T2* plasma focus has a small *RD*, consequently a large *ED* and cannot be completely fitted with the computed *RD*. Thus, a big RD drops the current a lot and strongly depletes the magnetic energy per unit mass at the end of the REGULAR radial phase. Hence a device with small RL produces a big RD and ends up with relatively less energy per unit mass at the end of the REGULAR phase when compared to a device with a big value of R_L. Therefore, a big *RD* generally tends to lead to a small *ED*; whereas a small *RD* is more conducive to lead to a larger *ED*.

From the above we may surmise that T1 plasma focus has a big *RD*, consequently a small *ED* and hence can be completely fitted using a model that computes only the *RD*, which is able to stretch its *RD* by stretching the model parameters until the large *RD* covers also the small *ED*. Moreover, energetically and mass-wise the fitting is correct. On the other hand *T2* plasma focus has a small *RD*, consequently a large *ED*. *T2* plasma focus cannot be completely fitted with the *RD* computed from the code, no matter how the model parameters are stretched. To fit the computed current trace to the measured current for *T2*, a phase 4a needs to be included into the model in order to progress the current dip beyond the small *RD* into the large *ED* part of the current dip.

Table 2 Classification of plasma focus machines (Ne operation)

PF name	L_0 (nH)	C_0 (μF)	I_{peak} (kA)	R_L	R_{EL}	RD dip (%)	Type
NX2 Ne	20	28	322	1.5	2.6	19	*T1*
UNUICTP Ne	110	30	178	15	26	2.5	*T2*

The Need of an Anomalus Resistance Term in the Lee Model

It is generally accepted [27] that after the regular dynamic phases ending in the formation of the plasma focus pinch, at the end of the pinch the system becomes unstable, develops a high 'anomalous' resistivity and breaks up. The overall processes to start this instability takes an exceedingly short time, the experimental observations indicate that the breakup time is far shorter than the 'regular' radial phases. This is evident for example in the streak photograph of Fig. 1 which shows that the break up time is less than the duration of the pinch which is measured as 30 ns after a duration of some 80 ns for the radial inward shock and reflected shock phases. There appears to be large number of competing instability processes [27], among which are some with exceedingly short time scales. Hence it appears reasonable to assume that the speed at which the plasma can convert the remnant inductive energy into anomalously resistive energy is ultimately limited by the time scales of the gross electrical components which have to supply the energy for the break-up processes.

From a careful study of measured waveforms of current and voltages, various sources have reported that the plasma anomalous resistive voltages are consistent with an 'anomalous' resistance of the order of 1Ω [15, 27]. Hence the (1/e) time scale (which is L/R) of current is estimated as 10 ns per 10 nH of inductance ($L_0 + L_a + L_{pinch}$); that is the time it takes the current to drop to some 36% limited by the lumped components of the circuit. Because inductive energy is proportional to I^2, this is also the time it would take for the inductive energy to drop to some 14%. On the other hand, the time it takes for inductive energy to drop to 55% $(\exp[-0.3])^2$ is some 3 ns per 10 nH. For a low L_0 (20–30 nH) plasma focus with this quantity of

inductance ($L_0 + L_a + L_{pinch}$) of around 40 nH this range of time (for inductive energy drop to 14–55%) is of the order of 12–40 ns. On the other hand for a high L_0 plasma focus with $L_0 = 120$ nH and the total inductance being 130 nH, this 14–55% inductive energy drop range could be some 40–130 ns. Thus, for a low L_0 system assuming a range of inductive energy drop down to 14–55%, we may estimate a relatively small *ED* region with small depth and timescale of the order of 12–40 ns. Whereas for a high L_0 system we expect a relatively high dip *ED* region with time scales of the order of 40–130 ns (for KSU PF shot 2: end RD to end AR1 $\sim$ 40 ns; end AR1 to end AR2 $\sim$ 80 ns; end AR2 to end AR3 $\sim$ 100 ns; not inconsistent with the above estimates).

Therefore a low L_0 system would have a small (in depth and in time) *ED* which can easily be merged into the larger (in depth and in time) *RD*; the whole current dip being capable of being treated as just the *RD*. On the other hand the high L_0 system would have an *E*D which is large (in both depth and time) when compared with the *RD*; hence the *ED* has to be separately treated by modelling a phase 4a.

One way to simulate the current *ED* is to assign the phase 4a period with an anomalous resistance term such as:

$$R = R_0[\exp(-t/t_2) - \exp(-t/t_1)] \quad (1)$$

where R_0 is of the order of 1Ω, t_1 is a characteristic time representative of the rise time of the anomalous resistance and t_2 is characteristic of the fall time of the anomalous resistance (Fig. 6).

We have applied this technique to the KSU current waveform (Fig. 5). We note that the computed *RD* does not follow the measured current dip which goes on to an *ED*. Following that first current dip in this particular case the dip continues in a second portion which is almost flat then followed by a third section which is less steep than the first dip but of slightly longer duration. We applied a resistance term to each of the three sections. We adjusted the parameters R_0, t_2 and t_1 for each of the section as well as a

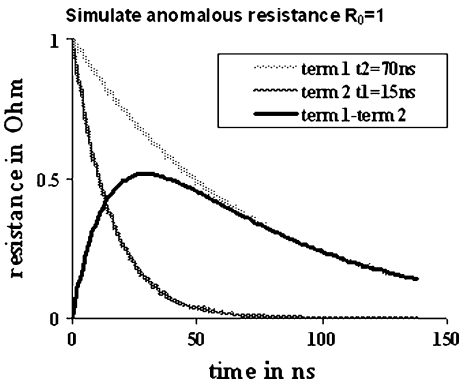

Fig. 6 Simulating anomalous resistance

Table 3 Anomalous resistances used for the fitting

ED	R_0 (Ω)	t_2(ns)	t_1 (ns)	Endfraction
Dip 1	1.0	70	15	0.53
Dip 2	0.2	70	40	0.4
Dip 3	0.5	70	25	1.0

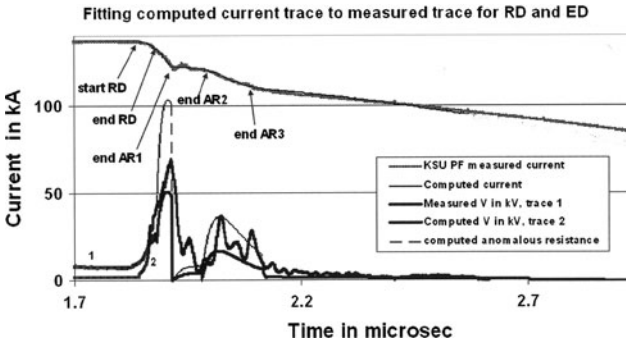

Fig. 7 Computed Current (dip region only and expanded to see details) fitted to measured current with inclusion of Phase 4a. Note that the computed current trace is fitted so well to the measured current trace that the two traces lie very closely on top of each other, these being the topmost traces (overlapping). Note also that the computed trace is stopped at 2.6 microsecond which is beyond the end of the AR3

fraction (*endfraction*) which terminates the term. The fitted parameters are as follows (Table 3):

With these parameters it is found that the computed current dip now fits the measured current dip all the way to the end of the current dip at 2.1 microsecond (See Fig. 7) and even beyond to 2.6 microsecond where the computation ends as we are not interested in the fitting beyond phase 4a. The fitting has involved the fitting of the *RD* followed by the *ED* of the first dip, then the second and third dips treated as *ED*'s each requiring a separate anomalous resistance function.

The resistance functions used for the fitting are also shown in Fig. 7 (dashed trace, with the resistance values magnified 200 times in order to be visible on the scale of Fig. 7). The computed voltage waveform is also shown (trace labeled 2) compared with the measured voltage waveform (trace labeled 1). The correspondence of the computed voltage waveform and the measured is seen clearly.

Conclusion

Plasma focus machines are classified into types *T1* and *T2*. A *T1* plasma focus has generally low static inductance L_0, has a large *RD*, small *ED* and can be completely fitted with the five-phase Lee model code using just regular radial

dynamics mechanisms. A *T2* plasma focus has generally high L_0, a small *RD* and a large *ED* and cannot be completely fitted with the 5-phase Lee model code; only the *RD* is fitted leaving a usually large *ED* not fitted. Additional distinguishing features as confirmed by numerical experiments include the ratio $R_{\mathrm{L}} = (L_0 + L_{\mathrm{a}})/L_{\mathrm{pinch}}$ and $R_{\mathrm{EL}} = (E_{\mathrm{L0}} + E_{\mathrm{La}})/E_{\mathrm{Lpinch}}$, these ratios being generally small for *T1* and large for *T2*. The explanation is a *T1* plasma focus with a small L_0 transfers energy efficiently through the regular dynamics as evidenced by the large *RD* current dip. At the end of the large *RD*, there is relatively little energy left that may be transferred to the instabilities. Moreover, the time constant governing this remnant energy transfer is only about 10 ns (taking the example of a $L_0 \sim$ 20–30 nH plasma focus). Thus, the smaller *ED* merges into the larger *RD* and can be 'absorbed' by the fitting process using model parameters. On the other hand a *T2* plasma focus has a small *RD* dip at the end of which there is a large amount of remnant inductive energy that may be transferred to instabilities with a time constant estimated in the range of 40 ns (for a plasma focus with $L_0 = 120$ nH). Thus, the *ED* occurring after the small *RD* is large in both dip depth as well as duration. Hence modelling just the *RD* would not be able to 'absorb' the larger *ED*. An attempt is made to model an instability phase 4a using fitted 'anomalous' resistance terms, one term for each major changing slope of measured current dip. In this manner, the computed current dip of the KSU plasma focus is completely fitted to the measured. In the process the resistance terms of the plasma focus are obtained. These resistance terms may then be used to examine instability mechanisms operating during those parts of the plasma focus forming the extended dips *ED*. The new six-phase model obtains the anomalous resistance functions that are needed to fit the instability phase. These anomalous resistance functions are experimental results derived from the measured current waveform and will be of use to throw more light on the types and extent of instabilities occurring after the regular dynamic phase.

References

1. S. Lee, in *Radiations in Plasmas*, vol. II, ed. by B.E. McNamara (World Scientific, Singapore, 1984), pp. 978–987
2. Lee S, *Radiative Dense Plasma Focus Computation Package*: RADPF, 2010 http://www.plasmafocus.net. http://www.plasmafocus.net/IPFS/modelpackage/File1RADPF.htm. http://www.plasmafocus.net/IPFS/modelpackage/File2Theory.pdf. http://www.plasmafocus.net/IPFS/modelpackage/UPF.htm
3. S. Lee, S.H. Saw, Appl. Phys. Lett. **92**(2), 021 503 (2008)
4. S. Lee, P. Lee, S.H. Saw, R.S. Rawat, Plasma Phys. Control. Fusion **50**(6), 065 012 (2008)
5. S.P. Chow, S. Lee, B.C. Tan, J. Plasma Phys. **8**, 21–31 (1972)
6. S.H. Saw, P.C.K. Lee, R.S. Rawat, S. Lee, IEEE Trans. Plasma Sci. **37**, 1276–1282 (2009)
7. S. Lee, R.S. Rawat, P. Lee, S.H. Saw, J. Appl. Phys. **106**, 023309 (2009)
8. S. Lee, Appl. Phys. Lett. **95**, 151503 (2009)
9. S. Lee, S.H. Saw, L. Soto, S.P. Moo, S.V. Springham, Plasma Phys. Control. Fusion **51**, 075006 (2009)
10. S. Lee, S.H. Saw, J. Fusion Energy **27**(4), 292–295 (2008)
11. S. Lee, Plasma Phys. Control. Fusion **50**(10), 105005 (2008)
12. S. Lee, S.H. Saw, P.C.K. Lee, R.S. Rawat, H. Schmidt, Appl. Phys. Lett. **92**, 11–111501 (2008)
13. M. Akel, Sh. Al-Hawat, S. Lee, J. Fusion Energy **28**, 355–363 (2009). doi:10.1007/s10894-009-9203-4
14. S. Lee, S.H. Saw, P. Lee, R.S. Rawat, Plasma Physi. Control. Fusion **51**, 105013 (2009)
15. T.Y. Tou, *Pinch Radius Ratio of the Plasma Focus*. PhD Thesis (p. 81) Universiti Malaya Kuala Lumpur, 1986
16. T.Y. Tou, S. Lee, K.H. Kwek, IEEE Trans. Plasma Sci. **17**(2), 311–315 (1989)
17. http://www.intimal.edu.my/school/fas/UFLF/
18. V. Rishi, R.S. Rawat, P. Lee, S. Lee, S.V. Springham, T.L. Tan, M. Krishnan, Phys. Lett. A **373**, 2568–2571 (2009)
19. S. Lee, T.Y. Tou, S.P. Moo, M.A. Eissa, A.V. Gholap, K.H. Kwek, S. Mulyodrono, A.J. Smith, S. Suryadi, W. Usada, M. Zakaullah, Am. J. Phys. **56**(1), 62–68 (1988)
20. A. Serban, S. Lee, J. Plasma Phys. **60**(1), pt. 1, 3–15 (1998)
21. M.H. Liu, X.P. Feng, S.V. Springham, S. Lee, IEEE Trans. Plasma Sci. **26**(2), 135–140 (1998)
22. S.V. Springham, S. Lee, M.S. Rafique, Plasma Phys. Control. Fusion **42**(10), 1023–1032 (2000)
23. M. Favre, S. Lee, S.P. Moo, C.S. Wong, Plasma Sourc. Sci. Tech. **1**, 122–125 (1992)
24. S.H. Saw, S. Lee, F. Roy, P.L. Chong, V. Vengadeswaran, S.S.M. Sidik, Y.W. Leong, A. Singh, Rev. Sci. Instrum. **81**, 053505 (2010)
25. S.L. Yap, S.H. Lee, L.K. Lim, C.S. Wong, in *Proceedings International Workshop on Plasma Computations and Applications (IWPCA2008),* ed. by S.S. Heoh et al. 14–15 July 2008 ISSN 165-0284. (INTI Publishing House Sdn Bhd, Malaysia, 2008), pp 51–54
26. A.E. Abdou et al., in *37th IEEE International Conference on Plasma Science ICOPS,* (session 6D) Norfolk, VA, USA, 20–24 June, 2010
27. A. Bernard et al., Moscow J. Phys. Soc. **8**, 93–170 (1998)
28. S. Lee, A. Serban, IEEE Trans. Plasma Sci. **24**, 1101 (1996)